Transp Porous Med (2010) 82:463–483
DOI 10.1007/s11242-009-9408-z

Cahn–Hilliard/Navier–Stokes Model for the Simulation of Three-Phase Flows

F. Boyer · C. Lapuerta · S. Minjeaud · B. Piar · M. Quintard

Received: 12 November 2008 / Accepted: 15 April 2009 / Published online: 7 May 2009
© Springer Science+Business Media B.V. 2009

Abstract In this article, we describe some aspects of the diffuse interface modelling of incompressible flows, composed of three immiscible components, without phase change. In the diffuse interface methods, system evolution is driven by the minimisation of a free energy. The originality of our approach, derived from the Cahn–Hilliard model, comes from the particular form of energy we proposed in Boyer and Lapuerta (M2AN Math Model Numer Anal, 40:653–987,2006), which, among other interesting properties, ensures consistency with the two-phase model. The modelling of three-phase flows is further completed by coupling the Cahn–Hilliard system and the Navier–Stokes equations where surface tensions are taken into account through volume capillary forces. These equations are discretized in time and space paying attention to the fact that most of the main properties of the original model (volume conservation and energy estimate) have to be maintained at the discrete level. An adaptive refinement method is finally used to obtain an accurate resolution of very thin moving internal layers, while limiting the total number of cells in the grids all along the simulation. Different

F. Boyer (✉)
Université Paul Cézanne, FST Saint-Jérôme, Case cour A, LATP, Avenue Escadrille Normandie-Niemen, 13397 Marseille Cedex 20, France
e-mail: fboyer@latp.univ-mrs.fr

C. Lapuerta · S. Minjeaud · B. Piar
Institut de Radioprotection et de Sûreté Nucléaire, Bat 702, BP3, 13115 Saint Paul lez Durance, France

C. Lapuerta
e-mail: celine.lapuerta@irsn.fr

S. Minjeaud
e-mail: sebastian.minjeaud@irsn.fr

B. Piar
e-mail: bruno.piar@irsn.fr

M. Quintard
Université de Toulouse; INPT, UPS; CNRS; UMR 5502; Institut de Mécanique des Fluides de Toulouse, Allée du Professeur Camille Soula, 31400 Toulouse, France
e-mail: Michel.Quintard@imft.fr

numerical results are given, from the validation case of the lens spreading between two phases (contact angles and pressure jumps), to the study of mass transfer through a liquid/liquid interface crossed by a single rising gas bubble. The numerical applications are performed with large ratio between densities and viscosities and three different surface tensions.

Keywords Cahn–Hilliard/Navier–Stokes model · Three phase flows · Local adaptive refinement

1 Introduction

Three-phase flows are encountered in many applications outside or within porous media. Their impact on many processes is very important. For instance, the correct understanding of three-phase flow (oil/gas/water) in petroleum engineering is crucial for the design of efficient recovery techniques. Similarly, the flow of non-aqueous phase liquid (NAPL) in the unsaturated zone determines the extent of the polluted zone and the future development of a pollution plume in the aquifer. The macro-scale modelling of three-phase flow in porous media is largely heuristic, based on generalized Darcy's laws. The correct modelling of pore-scale mechanisms, mostly through direct numerical simulations, is expected to bring a better understanding of the physics, and allow for better macro-scale models. Models accurately solving pore-scale three-phase flow problems without major restrictions are desperately needed. Many problems outside porous media are also of great practical importance. For instance, in nuclear safety, during a hypothetical major accident in a pressurized water reactor, the deterioration of the core can produce a stratified pool crossed by a bubbly flow. The mechanism of the entrainment of the heavy fluid in the light phase, induced by the bubbly flow can heavily modify heat transfers, whose intensities are crucial in the progression of the accident. This is the context of the works presented in this paper.

Direct simulations with diffuse interface models (see, for instance, the review in Anderson et al. 1998) in the case of two-phase flows have proven to be very useful to answer fundamental questions concerning the different occurring mechanisms (see, for examples, Bonometti and Magnaudet 2007; Fichot et al. 2007; Yue et al. 2004). Unfortunately, few numerical models are available to directly simulate three-phase flows. We can note the studies of Kim and co. who studied how to generalize the coupling between such multi-component Cahn–Hilliard models and the Navier–Stokes equations and how to implement efficient numerical solvers (see Kim et al. 2004; Kim and Lowengrub 2005; Kim 2007).

In this article, we propose diffuse interface modelling based on the Cahn–Hilliard approach for the study of incompressible flows, composed of three immiscible components. The construction of a free energy that has good properties is crucial to obtain a model able to simulate both two- and three-phase situations. Our approach ensures that there is no artificial apparition of one phase inside the interface between the other two. In order to describe the hydrodynamics of the mixture, the Cahn–Hilliard and the Navier–Stokes equations for incompressible flows are coupled. The formulation of the momentum equation, used in this article, is not classical and enables to control the kinetic energy. The interfacial surface tension forces are naturally taken into account through volume capillary forces. The details of the construction and the analysis of the three component Cahn–Hilliard model are given in Boyer and Lapuerta (2006).

A numerical difficulty in using diffuse interface approaches is to be able to get an accurate resolution of very thin moving internal layers. To address this question, we choose to use a refinement method called Conforming Hierarchical Adaptive Refinement MethodS

(CHARMS), initially developed by Krysl, Grinspun, Schröder in Krysl et al. (2003). The key feature of the method is performing basis functions (un-)refinement instead of cells (un-)refinement. We propose a new discretization for the Cahn–Hilliard/Navier–Stokes system based on the adaptive refinement method. Moreover, the discretization ensures that the kinetic energy does not blow up during simulations.

In this article, we propose a general description of the CH/NS model and of the discretizations used for the simulation of three-phase flows. The details of the analysis and the developments are given in Boyer and Lapuerta (2006); Boyer et al. (2009); Boyer and Minjeaud (2008, in preparation). We particularly point out here the most intricate aspects of the simulation of complex flows with large ratios between densities and viscosities of the phases. More precisely, we emphasize the necessity of a consistency property of the model with two-phase flow cases, of the control of the total energy of the system, of the exact volume conservation of each phase and finally, of the local adaptive refinement methods that let us achieve a very small interface thickness in the simulations. The outline of the article is as follows. In Sect. 2, after a brief introduction to the usual binary Cahn–Hilliard model, we present the general construction of a ternary model. The next section is devoted to the numerical schemes for the Cahn–Hilliard/Navier–Stokes system using the local adaptive refinement method. Finally, in the last section, two applications are presented: the partial and total spreading of the lens between two liquids and the gas bubble rising through two stratified fluid layers.

2 Three-Component Cahn–Hilliard/Navier–Stokes Model

In this section, we propose a general description of the ternary Cahn–Hilliard/Navier–Stokes model. We only briefly present here the main steps in the construction of the model, since the complete derivation and the analysis of this model are given in Boyer and Lapuerta (2006).

2.1 Introduction: Cahn–Hilliard Model

The Cahn–Hilliard approach consists of assuming that the interface thickness between two phases in a system is small but greater than the real physical one. One phase is described geometrically by a smooth function c_i, called 'order parameter', which is equal to 1 in the phase i and 0 outside, and which varies continuously in the interfaces between the phase i and the others (Fig. 1). From a mathematical point of view, this approach may be understood as a regularization of sharp interface models with small interfacial thickness Jacqmin (1999).

The system evolution is driven by the minimisation of a free energy. The two-component Cahn–Hilliard free energy is defined by

$$\mathcal{F}^{\text{diph}}_{\sigma,\varepsilon}(c) = \int_\Omega \left[\frac{12}{\varepsilon} F(c) + \frac{3}{4}\sigma\varepsilon|\nabla c|^2 \right], \tag{1}$$

with $F(c) = \sigma c^2(1-c)^2$. The first term is called 'bulk energy' and the function F, called the Cahn–Hilliard potential, has a classical double-well structure with two minima for $c = 0$ and $c = 1$ (Fig. 1) corresponding to the two pure phases. The bulk energy tends to reduce the interfacial zone width whereas the second term $|\nabla c|^2$, called capillary term, tends to increase it. In this definition, σ is the surface tension and ε is the interface thickness. From a numerical point of view, one of the main features of this model is that ε can be chosen larger than its theoretical value without modifying the capillary properties of the interfaces.

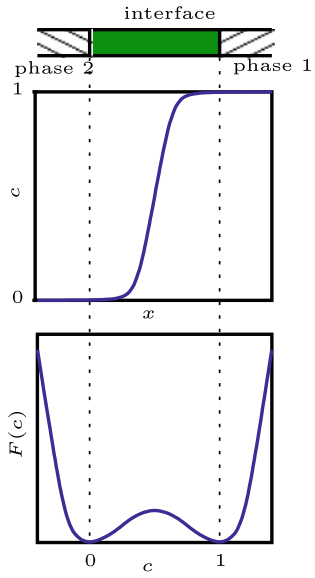

Fig. 1 Variation of the order parameter between two phases and double-well structure of the Cahn-Hilliard potential F

Note that the fourth-order polynomial formula for F is in fact an approximation of the actual value of the bulk free energy which is only valid, theoretically, in the vicinity of the critical point. The diffuse interface modelling in multiphase flows actually consists of using the same mathematical model outside its theoretical range of validity (see, for instance, Anderson et al. 1998; Kim and Lowengrub 2005; Lowengrub and Truskinovsky 1998) taking advantage of its interesting mathematical properties.

The evolution of the order parameter is driven by the gradient of the functional derivative $\mu = \frac{\delta \mathcal{F}^{\text{diph}}_{\sigma,\varepsilon}}{\delta c}$, called generalized chemical potential:

$$\begin{cases} \dfrac{\partial c}{\partial t} - \nabla \cdot (M_0 \nabla \mu) = 0, \\ \mu = \dfrac{\delta \mathcal{F}^{\text{diph}}_{\sigma,\varepsilon}}{\delta c} = -\dfrac{3}{2}\sigma\varepsilon\Delta c + 24\dfrac{\sigma}{\varepsilon}c(1-c)(1-2c). \end{cases} \tag{2}$$

The parameter M_0, called the mobility, is a diffusion coefficient which may depend on c. The boundary conditions are in general the homogeneous Neumann boundary conditions. For the potential μ, this condition ensures that there is no mass diffusion through the boundary. For the order parameter c, this condition implies that the interfaces are supposed to be orthogonal to the boundary of the computational domain. One interesting feature of Cahn–Hilliard models is that it is possible to consider non-homogeneous and non-linear Neumann conditions to model more general contact angles.

2.2 Construction of a Three-Component Model

Our aim is to generalise the diphasic Cahn–Hilliard model presented above for the simulation of three immiscible component flows, without phase change. We introduce three order parameters, c_1, c_2 and c_3, each representing the volume concentration of one component. As the three phases are supposed to be immiscible, we in fact look for a model which is able to simulate 'three times two phase situations'. Indeed, in expected applications, most

of the interfacial areas are only concerned with two phases and not with the third one. Of course, ternary points may exist but have to be thought as exceptional: a typical situation being the one of a gas bubble rising into a stratified two-fluid system, for which the physical problem is mainly diphasic, except when the bubble crosses the liquid–liquid interface. To this end, it is very important that the model used for three components enjoys a consistency property with the two-phase system. This precisely means that, in areas where only two phases among three are present in the system, the mathematical model should not artificially generate the appearance of the third phase. Consequently, our approach consists of building a mathematical model that satisfies the following constraints:

1. $\sum_{i=1}^{3} c_i = 1$ for each point and each time,
2. the equations satisfied by c_1, c_2 and c_3 should be formally identical,
3. the three-phase model should coincide with the two-phase model when only two phases are present (that is, if for instance, $c_3 = 0$ everywhere in the domain).

Remark 1 In particular, from a practical point of view, one of the order parameters, c_1, c_2 or c_3, will be eliminated *a posteriori* and the solution must not depend on the choice of the eliminated unknown. Therefore, only two coupled Cahn–Hilliard equations will be finally solved to save computational work.

2.2.1 Free Energy and Evolution Equations

In view of the diphasic case, we postulate that the free energy can be written as follows:

$$\mathcal{F}^{\text{triph}}_{\boldsymbol{\Sigma},\varepsilon}(c_1,c_2,c_3) = \int_\Omega \left[\frac{12}{\varepsilon} F(c_1,c_2,c_3) + \frac{3}{8}\varepsilon\Sigma_1|\nabla c_1|^2 + \frac{3}{8}\varepsilon\Sigma_2|\nabla c_2|^2 + \frac{3}{8}\varepsilon\Sigma_3|\nabla c_3|^2 \right], \tag{3}$$

with bulk energy F and three capillary terms.

The coefficients Σ_1, Σ_2, Σ_3 and the function F will be determined later and we first concentrate here on the evolution equations associated to this model, taking into account the constraint

$$\sum_{i=1}^{3} c_i = 1. \tag{4}$$

As in the diphasic case, the evolution of the order parameters is driven by the minimisation of the free energy. In order to ensure the constraint (4), a Lagrange multiplier technique is used. The Cahn–Hilliard equations we finally obtain are

$$\forall i \in \{1,2,3\}, \quad \begin{cases} \dfrac{\partial c_i}{\partial t} = \nabla \cdot \left(\dfrac{M_0}{\Sigma_i} \nabla \mu_i \right), \\ \mu_i = \dfrac{4\Sigma_T}{\varepsilon} \displaystyle\sum_{j \neq i} \left(\frac{1}{\Sigma_j} \left(\partial_i F(\mathbf{c}) - \partial_j F(\mathbf{c}) \right) \right) - \dfrac{3}{4}\varepsilon\Sigma_i \Delta c_i, \end{cases} \tag{5}$$

where the coefficient Σ_T is defined by $\frac{3}{\Sigma_T} = \frac{1}{\Sigma_1} + \frac{1}{\Sigma_2} + \frac{1}{\Sigma_3}$.

2.2.2 *Consistency with the Two-Phase Model*

In order to ensure the constraints described above, the model must satisfy two properties :

(P1) When a phase i is not present, the three-phase free energy is equal to the one of the two-phase model,
(P2) When a phase i is not present at initial time, the phase must not appear artificially during the evolution of the system.

In this case, we say that the model is *consistent* with the two-phase models.
Capillary terms: In order to satisfy the property (P1), we easily find that the capillary coefficients have to be taken as follows:

$$\Sigma_i = \sigma_{ij} + \sigma_{ik} - \sigma_{jk}, \tag{6}$$

where the surface tensions σ_{12}, σ_{13} and σ_{23} are given.

The coefficient $S_i = -\Sigma_i$ is called spreading parameter of the phase i at the interface between phases j and k Rowlinson and Widom (1982). If S_i is positive, the spreading is said to be total and if S_i is negative, it is said to be partial (see Sect. 4.1). It is interesting to notice here, and this will be enforced by the discussion in the sequel of the article, that the spreading coefficient appears as a key parameter in the proposed Cahn–Hilliard formulation. Indeed, there is an extensive literature that shows the importance of this parameter in the case of three-phase flow, especially for flow in porous media (see Keller and Chen 2003; Mani and Mohanty 1997).
Bulk energy: In view of the diphasic case, a natural bulk energy would be

$$\bar{F} = \sigma_{12} c_1^2 c_2^2 + \sigma_{13} c_1^2 c_3^2 + \sigma_{23} c_2^2 c_3^2. \tag{7}$$

This formula for $\bar{F}$ clearly degenerates into the diphasic potential $\sigma_{ij} c_i^2 (1 - c_i)^2$ if the order parameter c_k is zero (so that $c_j = 1 - c_i$), which is exactly property (P1). Unfortunately, the second property (P2) that we required is not satisfied by this ternary potential.

To illustrate this, we propose to visualise the map of the function $\bar{F}$ in barycentric coordinates (see Fig. 2). More precisely, we represent the Gibbs triangle where the vertices correspond to the three pure phases. The points located at the interior of the triangle represents physically admissible values of the concentration. We observe inside the triangle a local minimum of $\bar{F}$. Since the evolution of the system is driven by the minimisation of the total energy,

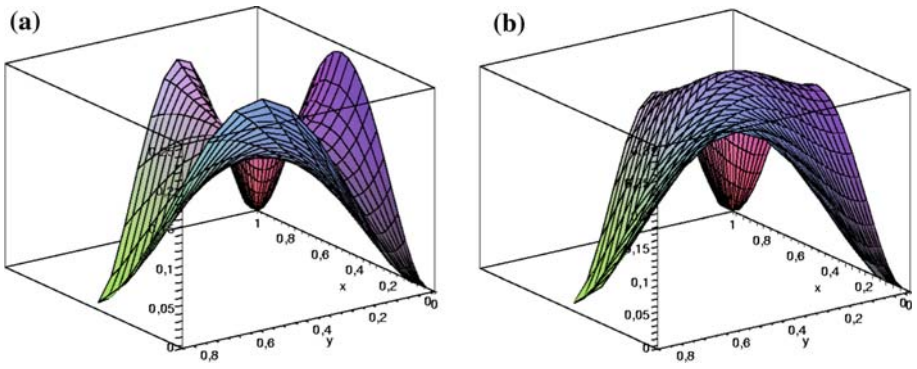

Fig. 2 Surfaces defined by $\bar{F}$ and F_Λ in barycentric coordinates. **a** $\bar{F}$, non consistent potential. **b** F_Λ, consistent potential

the choice of $\bar{F}$ will lead to non-physical apparition of one phase in the interface between the other two. Indeed, the least energy path between two vertices i, j (corresponding two pure phases) goes into the interior of the triangle since there is a local minimum. In the numerical illustrations given in Sect. 2.2.3, we will actually observe this unwanted behaviour and that the proposed expression for the potential F given below in (8) gives the expected results.

In Boyer and Lapuerta (2006), we show that, instead of $\bar{F}$, using the Cahn–Hilliard potential defined by

$$F_\Lambda = \sigma_{12}c_1^2c_2^2 + \sigma_{13}c_1^2c_3^2 + \sigma_{23}c_2^2c_3^2 + c_1c_2c_3(\Sigma_1c_1 + \Sigma_2c_2 + \Sigma_3c_3) + \Lambda c_1^2c_2^2c_3^2 \quad (8)$$

with $\Lambda \geq 0$, to be determined later, ensures the consistency properties (P1) and (P2). In Fig. 2, we see that the function has no minimum in the Gibbs triangle and that the least energy path between two vertices is exactly described by the corresponding edge of the triangle.

In practice, we note $F_\Lambda = F_0 + P$ where

$$\begin{aligned} F_0 &= \sigma_{12}c_1^2c_2^2 + \sigma_{13}c_1^2c_3^2 + \sigma_{23}c_2^2c_3^2 + c_1c_2c_3(\Sigma_1c_1 + \Sigma_2c_2 + \Sigma_3c_3), \\ P &= \Lambda c_1^2c_2^2c_3^2. \end{aligned} \quad (9)$$

Remark 2 Let us emphasize the fact that this formula for the potential has probably no true microscopic physical meaning. However, it satisfies the required mathematical properties for the final model to be consistent with the diphasic model, which is necessary for the simulation of three immiscible component flows as illustrated in Sect. 2.2.3. It can then be understood as a phenomenological extrapolation of the diphasic model to the ternary immiscible situation.

Properties: The analysis of the consistent ternary Cahn-Hilliard model is given in Boyer and Lapuerta (2006). In particular, we show that the system is mathematically well-posed if the parameter Λ is chosen large enough, and if we assume that the following conditions hold

$$\begin{cases} \Sigma_1\Sigma_2 + \Sigma_1\Sigma_3 + \Sigma_2\Sigma_3 > 0, \\ \Sigma_i + \Sigma_j > 0 \quad \text{for } i \neq j. \end{cases} \quad (10)$$

Notice that the second condition is always satisfied because, from (6), we deduce that

$$\Sigma_i + \Sigma_j = 2\sigma_{ij} > 0. \quad (11)$$

Moreover, the only condition on the sign of the coefficients Σ_i is the first equation in (10). In particular, the model is able to take into account for some total spreading situations (see Paragraph 4.1) provided that $\Lambda > 0$ is chosen large enough. In other situations (all coefficients $\Sigma_i > 0$), one can take $\Lambda = 0$.

2.2.3 Numerical Example: Consistent/Non-Consistent Model

In order to compare the consistent and non-consistent models, we used the classical problem of the simulation of the partial spreading of a liquid lens between two other liquid phases. At the equilibrium, the shape of the lens and the contact angles are well known (Young's relation). This example is studied in detail in Sect. 4.1.

For three different surface tensions,

$$\begin{aligned} \sigma_{\text{upper/lens}} &= 0.8, \\ \sigma_{\text{lower/lens}} &= 1.4, \\ \sigma_{\text{lower/upper}} &= 1, \end{aligned}$$

the numerical solution for the consistent model ($F = F_\Lambda$) is given in Fig. 3.

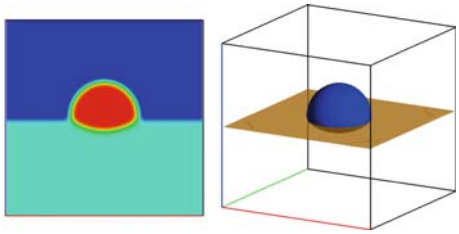

Fig. 3 Equilibrium state for the partial spreading of a lens between two stratified liquids

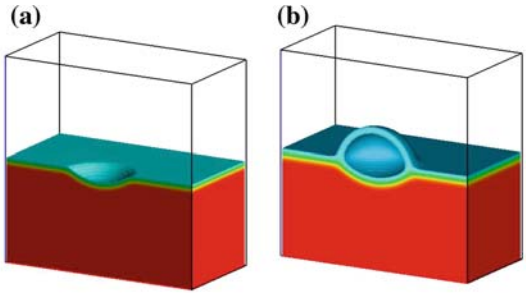

Fig. 4 Visualisation of the order parameter of the lower phase computed with a consistent (*left*) and a non-consistent (*right*) model. **a** Consistent model $F = F_\Lambda$. **b** Non-consistent model $F = \bar{F}$

In Fig. 4, we visualise the order parameter associated to the lower liquid phase. When we use the non-consistent model ($F = \bar{F}$), we observe that the lower phase appears artificially in the interface between the upper phase and the lens. This unsatisfactory behaviour is no more present when we use the potential $F = F_\Lambda$.

2.3 Coupling with the Hydrodynamics

In order to complete the modelling of three-phase incompressible flows, the Cahn–Hilliard system Boyer et al. (2009) is then coupled with Navier–Stokes equations (for more details, see Boyer 2002; Boyer and Lapuerta 2006; Jacqmin 1999; Kim 2005).

The velocity jump being zero between two phases, it is possible to define a unique velocity field that is smooth on the domain. In order to couple the equations, a convective term is added in the order parameters evolution equations and a capillary force,

$$F_{\text{ca}} = \mu_1 \nabla c_1 + \mu_2 \nabla c_2 + \mu_3 \nabla c_3, \tag{12}$$

is considered in the momentum balance. This force is a volumic approximation of the surface tension force (see Kim 2005). To this end, the Navier–Stokes equations are written as follows:

$$\begin{cases} \sqrt{\varrho}\dfrac{\partial}{\partial t}\left(\sqrt{\varrho}\mathbf{u}\right) + (\varrho\mathbf{u}\cdot\nabla)\,\mathbf{u} + \dfrac{\mathbf{u}}{2}\nabla\cdot(\varrho\mathbf{u}) - \nabla\cdot\left(\eta(\nabla\mathbf{u} + \nabla\mathbf{u}^t)\right) + \nabla p = \varrho g + F_{\text{ca}}, \\ \nabla\cdot\mathbf{u} = 0, \end{cases} \tag{13}$$

where the density ϱ and viscosity η are smooth functions that depend on the order parameters and satisfy, in the i-phase,

$$\varrho = \varrho_i, \quad \eta = \eta_i, \tag{14}$$

(details are given in Sect. 3.1).

Remark 3 If we try to write the evolution of the total energy of the system (kinetic energy + Cahn–Hilliard free energy), then we have to multiply the evolution equation of each c_i by μ_i and the Navier–Stokes equation by $\mathbf{u}$ and then sum up the results. We see that the free energy

creation by convection is exactly balanced with the kinetic energy creation by capillarity (see Jacqmin 1999).

This Navier–Stokes formulation is equivalent with the classical form

$$\begin{cases} \varrho \dfrac{\partial \mathbf{u}}{\partial t} + (\varrho \mathbf{u} \cdot \nabla)\, \mathbf{u} - \nabla \cdot \left(\eta(\nabla \mathbf{u} + \nabla \mathbf{u}^t)\right) + \nabla p = \varrho g + F_{\text{ca}}, \\ \nabla \cdot \mathbf{u} = 0, \end{cases} \tag{15}$$

if one uses the usual mass balance equation $\frac{\partial}{\partial t}\rho + \nabla \cdot (\varrho \mathbf{u}) = 0$.

However, in the diffuse interface modelling framework, the mass balance equation has a slightly different form since ϱ depends on c_1, c_2, c_3 which have their own evolution equation. In practice, the mass balance equation possesses an additional diffusion term (which comes from diffusion terms of (5)). Hence, the above formulation of the Navier–Stokes equations is strictly equivalent neither to the conservative formulation nor to the non-conservative formulation. Note that, in each phase, the mass balance is satisfied since the density is uniform $\varrho = \varrho_i$.

The reason for the choice of this formulation, initially proposed by Guermond and Quartapelle (2000) in the more usual context of variable-density incompressible single phase flows, is that it guarantees the control of the kinetic energy even if the mass balance equation is not of the classical form, or is not exactly satisfied (which can be the case in numerical computations). Indeed, multiplying the momentum equation by $\mathbf{u}$ and integrating on the domain, the time derivative form enables the time derivative kinetic energy to be obtained as

$$\int_\Omega \frac{\partial}{\partial t}\left(\sqrt{\varrho}\mathbf{u}\right) \cdot \sqrt{\varrho}\mathbf{u} = \frac{1}{2}\frac{d}{dt}\int_\Omega \varrho \mathbf{u}^2. \tag{16}$$

Furthermore, the convective contribution is zero

$$\int_\Omega \left[\mathbf{u} \cdot (\varrho \mathbf{u} \cdot \nabla)\, \mathbf{u} + \frac{\mathbf{u}^2}{2}\nabla \cdot (\varrho \mathbf{u})\right] = 0. \tag{17}$$

Indeed, assuming that $\mathbf{u} = 0$ on the boundary of the domain, then for any scalar function f, we have

$$\int_\Omega f\,(\varrho \mathbf{u} \cdot \nabla)\, f + \int_\Omega \frac{f^2}{2}\nabla \cdot (\varrho \mathbf{u}) = \frac{1}{2}\int_\Omega \nabla \cdot \left(\varrho \mathbf{u} f^2\right) = \frac{1}{2}\int_{\partial\Omega} \varrho f^2 \mathbf{u} \cdot n = 0. \tag{18}$$

In the Navier–Stokes equations, we use this calculation for each velocity component. The other terms in Eqs. 13 are written under a standard form.

For complex simulations with large ratios between densities and viscosities of the phases, the control of the total energy of the system is essential, even in the diphasic situation. We illustrate this point by comparing two numerical simulations of a bubble rising in a quiescent liquid. The properties of the two fluids are

- $\varrho_b = 0.1, \varrho_\ell = 7,800\ (\text{kg} \cdot \text{m}^{-3})$,
- $\eta_b = 7.3\ 10^{-5}, \eta_\ell = 0.001\ (\text{Pa} \cdot \text{s})$,
- $\sigma = 0.8\ \text{N} \cdot \text{m}^{-1}$.

If we use the standard form (15) of the momentum equation, then we observe in Fig. 5a that the kinetic energy blows up rapidly leading to instabilities that prevent the computation to be performed until the end. This unwanted behaviour is no more observed when we use the alternative formulation (13) (see Fig. 5b).

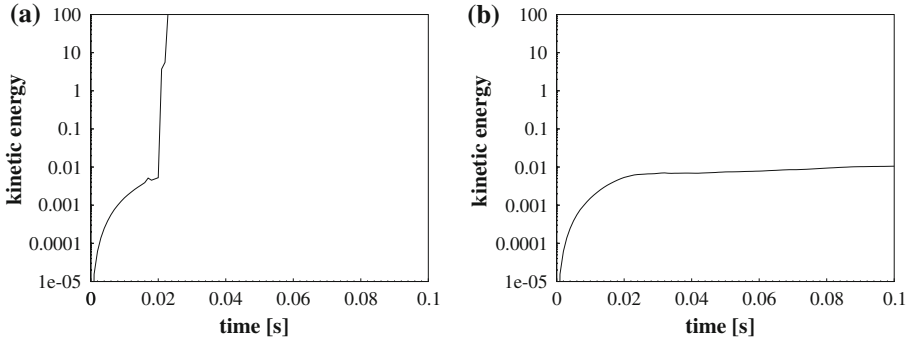

Fig. 5 Evolution of the kinetic energy during the bubble rising in a quiescent fluid. **a** Using the classical form of the momentum equation 15. **b** Using the alternative form of the momentum equation 13

3 Numerical Methods

A typical numerical issue in using diffuse interface approaches is to ensure accuracy of the resolution of very thin moving internal layers while limiting the total number of cells in the grid and thus the computational cost. The solution adopted here is the use of a local adaptive refinement method (CHARMS) initially proposed by Krysl et al. (2003), and more precisely described and studied in Boyer et al. (2009).

In this section, we give the time and spatial discretizations for the Cahn–Hilliard and Navier–Stokes (CH/NS) system, which ensures that the discrete total energy (the sum of the Cahn–Hilliard free energy and the kinetic energy) are controlled, at least for a small enough time step. Then, we propose a brief description of the CHARMS method and of its use for our applications.

The practical implementation has been performed using the software object-oriented component library PELICANS, developed at the french 'Institut de Radioprotection et de Sûreté Nucléaire' (IRSN) and distributed under the CeCILL-C license agreement (an adaptation of LGPL to the French law).

3.1 Time and Space Discretizations

In order to solve the CH/NS system, we use a Galerkin finite element method. The time discretization used is semi-implicit to split the Cahn–Hilliard and the Navier–Stokes problems within a time step as explained below. The resolution is performed using a Newton–Raphson method for the Cahn–Hilliard system and an Augmented Lagrangian method for Navier–Stokes equations.

Denoting by $\mathcal{V}_{\mathrm{x}}$ the finite element approximation space where we seek the discrete unknown x, the time marching in a time step is written as follows:

Let c_i^n, μ_i^n, $\mathbf{u}^n$ be known for $i = 1, 2$,

1. find $(c_1^{n+1}, c_2^{n+1}, \mu_1^{n+1}, \mu_2^{n+1}) \in (\mathcal{V}_{c,\mu})^4$ such that $\forall \nu \in \mathcal{V}_{c,\mu}$, we have for $i = 1, 2$

$$\int_\Omega \frac{c_i^{n+1} - c_i^n}{\Delta t}\nu + \int_\Omega \frac{M_0^n}{\Sigma_i}\nabla\mu_i^{n+1}\cdot\nabla\nu + \int_\Omega \mathbf{u}^n\cdot\nabla c^{n+1}\nu = 0, \tag{19}$$

$$\int_\Omega \mu_i^{n+1}\nu = \int_\Omega D_i(\mathbf{c}^{n+1}, \mathbf{c}^n)\nu + \int_\Omega \frac{3}{4}\Sigma_i\varepsilon\nabla c_i^{n+1}\cdot\nabla\nu. \tag{20}$$

with $D_i(\mathbf{c}^{n+1},\mathbf{c}^n) = \dfrac{4\Sigma_T}{\varepsilon}\displaystyle\sum_{j\neq i}\left(\frac{1}{\Sigma_j}\left(d_i(\mathbf{c}^{n+1},\mathbf{c}^n)-d_j(\mathbf{c}^{n+1},\mathbf{c}^n)\right)\right)$, where d_i represents a semi-implicit discretization of $\partial_{c_i}F_\Lambda$ defined by

$$d_i(\mathbf{c}^{n+1},\mathbf{c}^n) = \partial_i F_0(\mathbf{c}^{n+1}) + \frac{2}{3}\Lambda c_i^{n+1}\left[(c_j^n)^2(c_k^n)^2 + \frac{1}{2}(c_j^{n+1})^2(c_k^n)^2 + \frac{1}{2}(c_j^n)^2(c_k^{n+1})^2 + (c_j^{n+1})^2(c_k^{n+1})^2\right]. \quad (21)$$

2. Using c_i^{n+1} and μ_i^{n+1} $(i=1,2)$, compute c_3^{n+1}, μ_3^{n+1}, $F_{\text{ca}}^{n+1}=\sum_{i=1}^3\mu_i^{n+1}\nabla c_i^{n+1}$, ϱ^{n+1} and η^{n+1}.
3. Find $\mathbf{u}^{n+1}\in\mathcal{V}_\mathbf{u}$ and $p^{n+1}\in\mathcal{V}_p$ such that $\forall\mathbf{v}\in\mathcal{V}_\mathbf{u}$ and $\forall q\in\mathcal{V}_p$

$$\int_\Omega \sqrt{\varrho^{n+1}}\frac{\sqrt{\varrho^{n+1}}\mathbf{u}^{n+1}-\sqrt{\varrho^n}\mathbf{u}^n}{\Delta t}\cdot\mathbf{v} + \int_\Omega 2\eta^{n+1}D(\mathbf{u}^{n+1}):\nabla\mathbf{v} + \frac{1}{2}\int_\Omega\left(\varrho^{n+1}(\mathbf{u}^n\cdot\nabla)\mathbf{u}^{n+1}\right)\cdot\mathbf{v} - \frac{1}{2}\int_\Omega\left(\varrho^{n+1}(\mathbf{u}^n\cdot\nabla)\mathbf{v}\right)\cdot\mathbf{u}^{n+1} = \int_\Omega p^{n+1}\nabla\cdot\mathbf{v} + \int_\Omega(F_{\text{ca}}^{n+1}+\varrho^{n+1}g)\cdot\mathbf{v}, \quad (22)$$

$$\int_\Omega \nabla\cdot\mathbf{u}^{n+1}q = 0. \quad (23)$$

In (20), the time discretization $D_i(\mathbf{c}^{n+1},\mathbf{c}^n)$ of the non-linear terms (defined in (21)) is semi-implicit to ensure the control of the discrete Cahn–Hilliard free energy. Indeed, a separate study of the pure Cahn–Hilliard system (19)–(20) (i.e. without convective terms, $\mathbf{u}^n=0$) shows that the discrete free energy control is mandatory to prove the existence of the approximate solution and its convergence towards the solution of the initial problem. If this energy is not controlled, we observed cases where the Newton method does not converge. Other possible choices for the time discretizations d_i and the analysis of corresponding schemes are given in Boyer and Minjeaud (2008, in preparation).

In practice, the mobility coefficient M_0^n depends on order parameters at time t^n and is zero outside the interfaces: it is said to be degenerate. This has the effect of limiting diffusion outside the interface due to the pure Cahn–Hilliard equations and keeping the spatial localisation of the interfaces all along the simulations.

In order to ensure the conservation of the total volume of each constituent, we use the same element for the pressure as for the order parameters and the chemical potentials that is $\mathcal{V}_c=\mathcal{V}_\mu=\mathcal{V}_p$. Indeed, in that case, we have

$$\int_\Omega\frac{c_i^{n+1}-c_i^n}{\Delta t} = -\int_\Omega\mathbf{u}^n\cdot\nabla c_i^{n+1} = \int_\Omega c_i^{n+1}\nabla\cdot\mathbf{u}^n. \quad (24)$$

The last integral is zero thanks to the discrete incompressibility constraint (23) provided that c_i^{n+1} belongs to the pressure approximation space. In the numerical examples given in Sect. 4, the velocity is discretized using the $\mathbb{Q}_2$ element and the other fields using the $\mathbb{Q}_1$ element, which leads to an inf-sup stable numerical method.

In (22), the convective terms,

$$\int_\Omega \left(\varrho^{n+1}\left(\mathbf{u}^n\cdot\nabla\right)\mathbf{u}^{n+1}\right)\cdot\mathbf{v}+\int_\Omega \frac{\mathbf{u}^{n+1}\cdot\mathbf{v}}{2}\nabla\cdot(\varrho^{n+1}\mathbf{u}^n),$$

are written under the form

$$\frac{1}{2}\int_\Omega \left(\varrho^{n+1}(\mathbf{u}^n\cdot\nabla)\mathbf{u}^{n+1}\right)\cdot\mathbf{v}-\frac{1}{2}\int_\Omega \left(\varrho^{n+1}(\mathbf{u}^n\cdot\nabla)\mathbf{v}\right)\cdot\mathbf{u}^{n+1}.$$

In this formulation, the contribution of the convective terms in the kinetic energy balance equation is zero even though the numerical integrations for the finite element method are not exact.

The functions ϱ^{n+1} and η^{n+1} are defined by

$$\begin{aligned}\varrho^{n+1} &= (\varrho_1-\varrho_3)H_e(c_1^{n+1}-0.5)+(\varrho_2-\varrho_3)H_e(c_2^{n+1}-0.5)+\varrho_3,\\ \eta^{n+1} &= (\eta_1-\eta_3)H_e(c_1^{n+1}-0.5)+(\eta_2-\eta_3)H_e(c_2^{n+1}-0.5)+\eta_3,\end{aligned}\tag{25}$$

where H_e is a smooth approximation of the Heaviside function. Contrary to the arithmetic or harmonic averages used in the literature, this relation (25) enables to preserve the values ϱ_i and η_i in the phase i even though c_i is not exactly 1 due to numerical errors. Hence, this averaging technique avoids additional numerical errors, which appear to be critical in particular when there are large ratios between densities and viscosities of the phases.

3.2 Local Adaptive Refinement

In the finite element method, basis functions have a small support in comparison to the size of the domain. The idea is to use basis functions with increasingly small support around the smeared interfaces. The basic principle of the CHARMS method is to refine/unrefine primarily basis functions and not directly the cells.

The study of this method and its application to Cahn–Hilliard systems are given in detail in Boyer et al. (2009). We only recall next the main features of the method.

3.2.1 Adaptation Procedure

Consider an initial conforming grid (possibly unstructured) together with its finite elements structure. A conceptual hierarchy of nested grids is defined by successive divisions of cells into cells of the same type obtained by uniformly applying the same subdivision pattern. We obtain a sequence of Lagrange conformal finite element spaces X_j, with the property that each basis function at a given level j can be written as a linear combination of some basis functions of the immediate finer level $j+1$:

$$X_j\subset X_{j+1}\quad\Rightarrow\quad\varphi_k^j=\sum_l \beta_{k,l}^{j+1}\varphi_l^{j+1},$$

leading to a Child/Parent relationship,

$$\beta_{k,l}^{j+1}\neq 0\Leftrightarrow\varphi_k^j\text{is a }\textit{parent}\text{ of }\varphi_l^{j+1}\Leftrightarrow\varphi_l^{j+1}\text{ is a }\textit{child}\text{ of }\varphi_k^j.$$

Since the supports of basis functions are small, most of the coefficients $\beta_{k,l}^{j+1}$ are zero. Within a set of basis functions, the refinement (resp. unrefinement) of a parent is then defined by the

addition (resp. removal) of all its children. Geometric cells are accordingly split and coarsened, leading to nonconforming grids, but their role is limited to the integration domains and support of the basis functions which, more importantly, span conforming finite element spaces.

3.2.2 Time Marching and Grid Construction

For the discrete problem CH/NS proposed in Paragraph 3.1, we use the CHARMS method that involves few modifications in particular for the finite element approximation spaces.

In a time step, from the solution obtained at the previous time t^n, we refine or unrefine the basis functions that belong to $\mathcal{V}^n$ using a given criterion (a criterion for the Cahn–Hilliard/Navier–Stokes applications is given in the following Paragraph 3.2.3). This stage enables to define the new finite element approximation space $\mathcal{V}^{n+1}$ in which we search the solution at time t^{n+1}. The spaces $\mathcal{V}^{n+1}$ differ, in general, from the approximation space at time t^n. Notice that these spaces do not necessarily have the same dimensions (the grids may be different at each time step).

This method implies that in the variational formulations, some integrals contain basis functions that belong to two distinct approximation spaces $\mathcal{V}^{n+1}$ and $\mathcal{V}^n$. For example, we have to cope with the following integral

$$\int_\Omega \frac{c_{ih}^n}{\Delta t} v^{n+1}, \quad \text{with } c_{ih}^n \in \mathcal{V}^n, \quad \text{and} \quad v^{n+1} \in \mathcal{V}^{n+1}.$$

In order to compute these terms, the grid is built in such a way that each basis function belonging to either $\mathcal{V}^n$ or $\mathcal{V}^{n+1}$, is expressed as a polynomial function on each cell (the basis function is not piecewise defined on a cell). Thus, if one uses suitable quadrature rules, such integrals can be computed exactly. This method avoids, in particular, the use of intricate transfer operators between the grids.

3.2.3 Refinement/Unrefinement Criterion

In order to build $\mathcal{V}^{n+1}$ from $\mathcal{V}^n$, we need to define a refinement/unrefinement criterion. For our applications, we want to refine in the interface zone (that is where the order parameters have important variations) and to unrefine away from the interfaces. This strategy is justified by the fact that, in our applications, the flow is not turbulent, and therefore, the small scales structures of the solution are only located at the interfaces. For other applications considering more turbulent flows, it is possible to adapt the refinement/unrefinement criterion to capture more complex hydrodynamic phenomenon.

As a consequence, we need to introduce an indicator measuring whether or not a given cell (resp. basis function) lies near the interfaces. The cell indicator is defined at time t^n by

$$\eta_K = \max\left(\frac{1}{|K|}\int_K c_1^n, \frac{1}{|K|}\int_K c_2^n, \frac{1}{|K|}\int_K c_3^n\right). \tag{26}$$

This cell indicator can be interpreted as follows:

- $\eta_K = 1$ means that the cell K is completely filled with one of the bulk phases.
- $\eta_K < 1$ means that the cell K contains an interface.

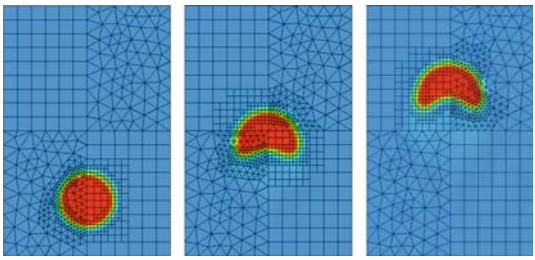

Fig. 6 Use of different finite elements ($\mathbb{P}_1$ and $\mathbb{Q}_1$)

Using the cell indicator, we can deduce a criterion for deciding whether or not a given basis function $\varphi \in \mathcal{V}^n$ may be (un-)refined. We use a volume weighted average of η_K over the support of φ:

$$\eta_\varphi = \frac{1}{|\text{supp}[\varphi]|} \sum_{K \cap \text{supp}[\varphi] \neq \emptyset} |K| \eta_K .$$

Given an expected cell size $h_{\text{interface}}$ for the interface neighbourhood, the two following criteria let us decide if a basis function φ has to be refined or unrefined:

– Refinement criterion:

$$\eta_\varphi < 0.90 \quad \text{and} \quad \text{diam}(K) > h_{\text{interface}} \quad \text{for at least one cell} K \subset \text{supp}[\varphi].$$

– Unrefinement criterion:

$$\eta_\varphi > 0.95.$$

In practice, $h_{\text{interface}}$ is chosen in such a way that each interface contains approximately three cells, that is $3h_{\text{interface}} \approx \varepsilon$.

3.2.4 Summary

The CHARMS method presents the following advantages:

– there is no modification of the discrete problem due to the mesh adaptation,
– the possible geometric non-conformity of the adapted meshes are implicitly handled,
– there is no specific treatment due to particular Lagrange finite elements ($\mathbb{P}_1, \mathbb{Q}_1$ see Fig. 6),
– all the procedure is independent of the space dimension (see Fig. 7),
– no need of transfer operators for fields defined on two distinct refined grids.

The use of adaptive local refinement enables us to choose an interface thickness ε very small while conserving a reasonable number of cells as we can see on Fig. 8 in the case of a rising gas bubble (this application is studied in Sect. 4.2)

4 Applications

In this section, we present two applications: the one of a lens spreading between two different liquids and the one of a gas bubble rising in two stratified liquid layers.

The computations are performed in axisymmetric 3D geometry using local adaptive refinement as described above.

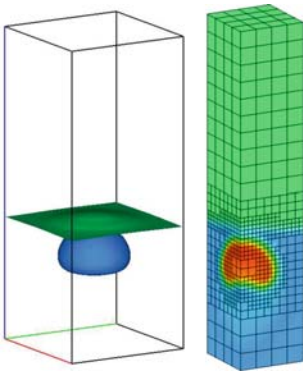

Fig. 7 Example of adaptive local refinement in 3D

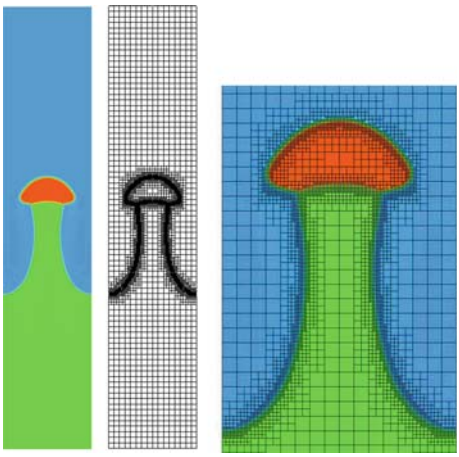

Fig. 8 Rising gas bubble in a stratified two-liquid geometry using local adaptive refinement

4.1 Spreading Lens between Two Stratified Liquid Layers

In this section, we show that the Cahn–Hilliard/Navier–Stokes model enables the accurate computation of contact angles and pressure jumps in the case of the partial spreading of a lens, and also the simulation of total spreading situations. In these numerical results, gravity effects are not taken into account since we are only interested in the computation of capillary effects.

4.1.1 Partial Spreading - Laplace's Law

At equilibrium, the positions of the interfaces are known: the shape of the lens is the intersection of two spherical caps. The contact angles depend on the three surface tensions as given by the Young's relation (see Fig. 9).

In Fig. 10, we present numerical solutions for different surface tension values. The white zone corresponds to the diffuse interface. We obtain a very good agreement with the theoretical solution (black solid line on the figure).

At the equilibrium, if there are no external forces, the theoretical velocity is zero and the pressures are uniform in each phase. The pressure jump between two phases is given by the

Young's relation :

$$\frac{\sin\theta_1}{\sigma_{23}} = \frac{\sin\theta_2}{\sigma_{13}} = \frac{\sin\theta_3}{\sigma_{12}}.$$

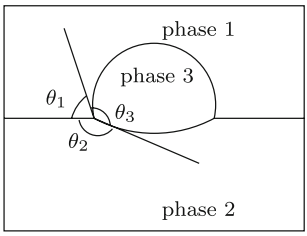

Fig. 9 Shape of the lens at equilibrium

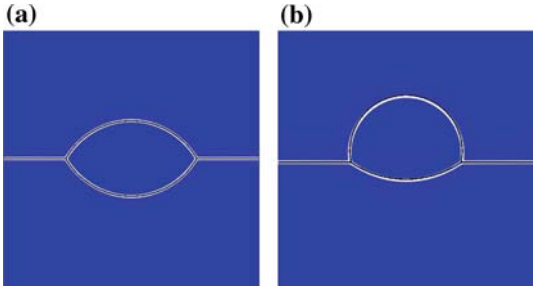

Fig. 10 Equilibrium states obtained numerically for different surface tensions (σ_{12}; σ_{13}; σ_{23}). **a** (1; 1; 1). **b** (1; 0.8; 1.4)

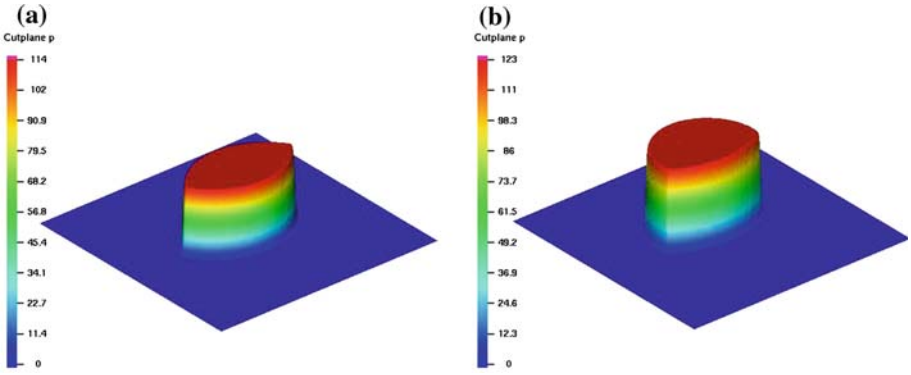

Fig. 11 Pressure jump for different surface tensions (σ_{12}; σ_{13}; σ_{23}). **a** (1; 1; 1). **b** (1; 0.8; 1.4)

Laplace's law and is written as

$$p_i - p_j = 2\frac{\sigma_{ij}}{r_{ij}} \tag{27}$$

where r_{ij} is the radius of the curvature of the interface between the phases i and j. In the present case, this leads to

$$\begin{cases} p_1 = p_2, \\ 2\dfrac{\sigma_{13}}{r_{13}} = p_3 - p_1 = p_3 - p_2 = 2\dfrac{\sigma_{23}}{r_{23}}. \end{cases} \tag{28}$$

In Fig. 11 and in Table 1, we can see that the Cahn–Hilliard/Navier–Stokes model enables the accurate computation of the pressure jump for different surface tensions values.

In our computations, the velocity is not zero but very small. We observe parasitic currents, which are a common problem for methods where the surface tension force is approximated

Table 1 Relative error of the pressure jump for different surface tensions

$(\sigma_{12};\sigma_{13};\sigma_{23})$	Theoretical pressure jump	Numerical pressure jump	Relative error
(1; 1; 1)	113.101	113.59	0.453%
(1; 0.8; 1.4)	121.644	122.9	1.03%

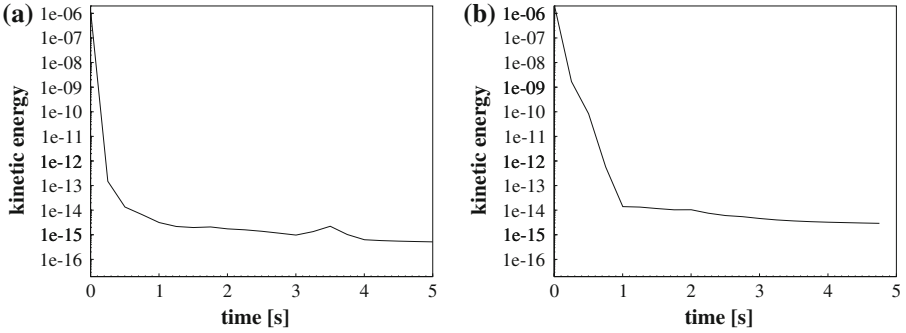

Fig. 12 Evolution of the kinetic energy for different surface tensions $(\sigma_{12};\sigma_{13};\sigma_{23})$. **a** (1; 1; 1). **b** (1; 0.8; 1.4)

by a volume force (see Jamet et al. 2002). These spurious currents decrease when the system tends to the equilibrium state. Indeed, in Fig. 12, we can see that the kinetic energy decreases during time.

4.1.2 Total Spreading

In the case where one of the spreading parameters S_i is positive (that is $\Sigma_i < 0$), the spreading is said to be total. Two configurations of total spreading are simulated: when the lens spreads between the liquids and when the upper liquid spreads between the lens and the lower liquid. The surface tensions are

- for the lens spreading: $(\sigma_{12};\sigma_{13};\sigma_{23}) = (3; 1; 1)$, $\Sigma_3 < 0$,
- for the upper phase spreading: $(\sigma_{12};\sigma_{13};\sigma_{23}) = (1; 1; 3)$, $\Sigma_1 < 0$.

We can see in Fig. 13 that in both cases, the phase spreads in such a way that the triple points disappear. Then, the system tends to the equilibrium state: the interfaces are finally plane or spherical.

4.2 Behaviour of a Bubble in Two Stratified Layers

During a gas bubble rise in a two stratified liquid layers configuration, the bubble can either remain captured in the interface, or can penetrate in the lighter phase and possibly entrain the heavy phase. In Greene et al. (1988, 1991), the authors suggest two criteria on the bubble volume to predict the bubble penetration and the entrainment phenomenon. These criteria, based on a macroscopic balance between buoyancy and surface tension forces, have been validated experimentally. The physical parameters we used are given in Table 2. This test case confirms that the model and the numerical method we proposed are able to simulate three-phase flows with large density and viscosity ratios with a good qualitative and quantitative agreement with theoretical results.

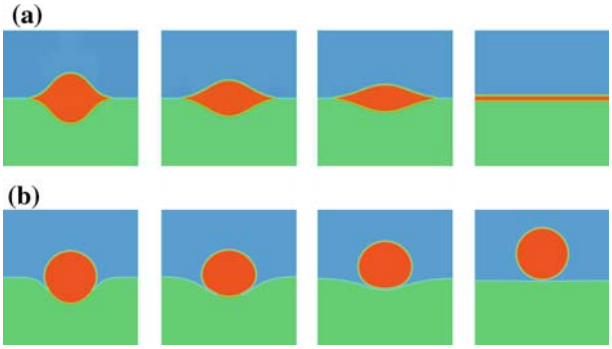

Fig. 13 Evolution of the interface for total spreading situation. **a** $(\sigma_{12};\sigma_{13};\sigma_{23}) = (3;1;1)$. **b** $(\sigma_{12};\sigma_{13};\sigma_{23}) = (1;1;3)$

Table 2 Physical properties

Surface tension ($\mathrm{N}\cdot\mathrm{m}^{-1}$)	
$\sigma_{\mathrm{gas-liquid}}$	0.07
$\sigma_{\mathrm{liquid-liquid}}$	0.05
Density ($\mathrm{kg}\cdot\mathrm{m}^{-3}$)	
Bubble c_1	1
Heavy liquid c_2	1,200
Light liquid c_3	1,000
Viscosity ($\mathrm{Pa}\cdot\mathrm{s}$)	
Bubble c_1	10^{-4}
Heavy liquid c_2	0.15
Light liquid c_3	0.1

We are interested here in the first criterion which predicts the bubble penetration if its volume V is greater than:

$$V_p = \left(\frac{2\pi \left(\frac{3}{4\pi}\right)^{\frac{1}{3}} \sigma_{23}}{(\varrho_3 - \varrho_1) g} \right)^{\frac{3}{2}} \simeq 8.87\ 10^{-8}\,\mathrm{m}^3,$$

i.e., for a bubble radius greater than $r_p \simeq 2.76\ 10^{-3}$ m. The numerical study gives $r_p^{\mathrm{num}} \simeq 2.5\ 10^{-3}$ m, which is in agreement with the criterion (see Fig. 14).

In the entrainment situations, the authors of Greene et al. (1991) experimentally studied the entrained volume of a heavy fluid into a light fluid when densities and viscosities vary. We propose to find these behaviours qualitatively by computing the quantity of the heavy liquid that is above the initial liquid–liquid interface position. In our study, the simulation with a bubble radius of $r = 8$ mm is considered as the reference case (see Fig. 15, circled marks in Fig. 16). The physical properties are the same as the previous ones.

Our results are in agreement with experiments: we observe an increase of the quantity of entrained volume when the light liquid density increases (see Fig. 16) and a decrease of the entrained volume when the viscosities and the heavy liquid density increase (see Fig. 16a, c and d).

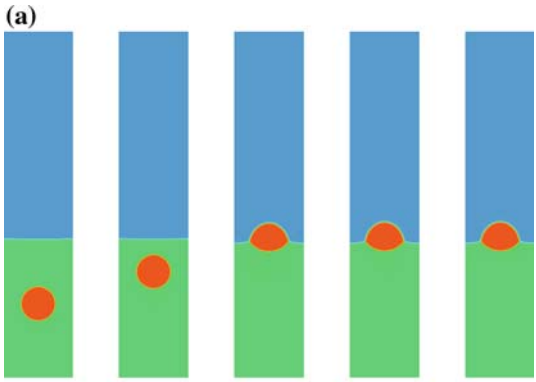

Fig. 14 Bubble rising in two stratified layers.
a $r = 0.002\,\mathrm{m} < r_p$.
b $r = 0.0029\,\mathrm{m} > r_p$

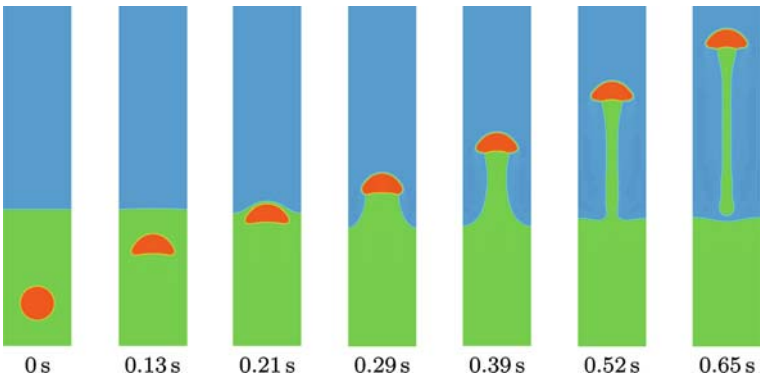

Fig. 15 Entrainment of the heavy liquid during the bubble rising with a radius $r = 8$mm

5 Conclusion

In this article, we described a Cahn–Hilliard/Navier–Stokes model for the simulation of incompressible flows composed of three immiscible components, with no phase change. The model is consistent with the two-phase model: there is no artificial apparition of the third phase in the interface between the other two. Moreover, the model is able to simulate

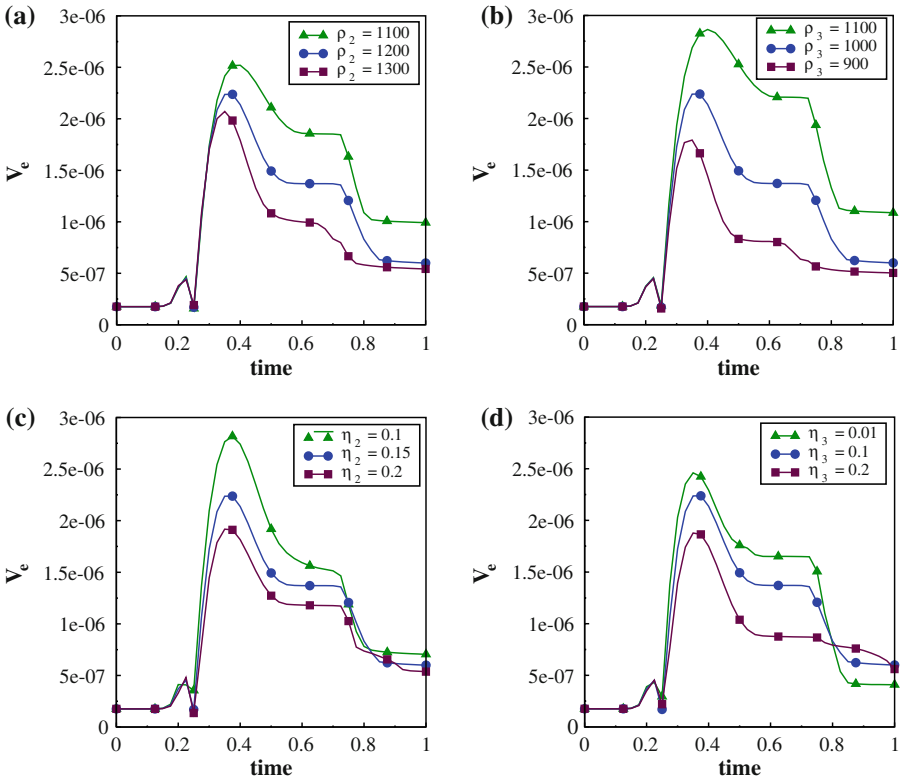

Fig. 16 Evolution of the entrained volume V_e of the heavy liquid in the light liquid. **a** Impact of the heavy liquid density. **b** Impact of the light liquid density. **c** Impact of the heavy liquid viscosity. **d** Impact of the light liquid viscosity

flows with a large ratio between the densities and the viscosities, with three different surface tensions and it takes into account total spreading situations.

The local adaptive refinement method enables us to simulate thin interfaces and have an accurate resolution in the interfacial zone. Finally, to compute 3D flows, it is necessary to use efficient linear solvers. In this context, a possible strategy is to use the multi-level structure naturally obtained by the local refinement algorithm to build multigrid preconditioners. Such a methodology and corresponding numerical results are described in Boyer et al. (2009).

In further studies, we will concentrate on the precise mathematical study of the full numerical method including the coupling between the Cahn–Hilliard and Navier–Stokes equations and the adaptive local refinement method.

References

Anderson, D.M., McFadden, G.B., Wheeler, A.A.: Diffuse-interface methods in fluid mechanics. Annu. Rev. Fluid Mech. **30**, 139–165 (1998)

Bonometti, T., Magnaudet, J.: An interface-capturing method for incompressible two-phase flows. Validation and application to bubble dynamics. Int. J. Multiph. Flow **33**, 109–133 (2007)

Boyer, F.: A theoretical and numerical model for the study of incompressible mixture flows. Comput. Fluids **31**, 41–68 (2002)
Boyer, F., Lapuerta, C.: Study of a three component Cahn-Hilliard flow model. M2AN, Math. Model. Numer. Anal. **40**, 653–687 (2006)
Boyer, F., Minjeaud, S.: Numerical schemes for a three component Cahn-Hilliard model, in preparation (2008)
Boyer, F., Lapuerta, C., Minjeaud, S., Piar, B.: A multigrid method with local adaptive refinement, application to a ternary Cahn-Hilliard model. ESAIM: Proc. (2009)
Fichot, F., Meekunnasombat, P., Belloni, J., Duval, F., Garcia, A., Quintard, M.: Two-phase flows in porous media: Prediction of pressure drops using a diffuse interface mathematical description. Nucl. Eng. Des. **237**, 1887–1898 (2007)
Greene, G.A., Chen, J.C., Conlin, M.T.: Onset of entrainment between immiscible liquid layers due to rising gas bubbles. Int. J. Heat Mass Transf. **31**, 1309–1317 (1988)
Greene, G.A., Chen, J.C., Conlin, M.T.: Bubble induced entrainment between stratified liquid layers. Int. J. Heat Mass Transf. **34**, 149–157 (1991)
Guermond, J.-L., Quartapelle, L.: A projection FEM for variable density incompressible flows. J. Comput. Phys. **165**, 167–188 (2000)
Jacqmin, D.: Calculation of two-phase Navier-Stokes flows using phase-field modelling. J. Comput. Phys. **155**, 96–127 (1999)
Jamet, D., Torres, D., Brackbill, J.U.: On the theory and computation of surface tension: the elimination of parasitic currents through energy conservation in the second-gradient method. J. Comput. Phys. **182**, 262–276 (2002)
Keller, A.A., Chen, M.: Effect of spreading coefficient on three-phase relative permeability of NAPL. Water Resour. Res. **39**, 1288 (2003)
Kim, J.: A continuous surface tension force formulation for diffuse-interface models. J. Comput. Phys. **204**, 784–804 (2005)
Kim, J., Lowengrub, J.: Phase field modeling and simulation of three-phase flows. Int. Free Bound. **7**, 435–466 (2005)
Kim, J.: Phase field computations for ternary fluid flows. Comput. Methods Appl. Mech. Eng. **196**, 45–48 (2007)
Kim, J., Kang, K., Lowengrub, J.: Conservative multigrid methods for ternary Cahn-Hilliard systems. Commun. Math. Sci. **2**, 53–77 (2004)
Krysl, P., Grinspun, E., Schröder, P.: Natural hierarchical refinement for finite element methods. Int. J. Numer. Meth. Eng. **56**, 1109–1124 (2003)
Lowengrub, J., Truskinovsky, L.: Quasi-incompressible Cahn-Hilliard fluids and topological transitions. Proc. R. Soc. Lond. A **454**, 2617–2654 (1998)
Mani, V., Mohanty, K.K.: Effect of the spreading coefficient on three-phase flow in porous media. J. Colloid Interf. Sci. **187**, 45–56 (1997)
PELICANS, Collaborative Development Environment: https://gforge.irsn.fr/gf/project/pelicans/
Rowlinson, J.S., Widom, B.: Molecular Theory of Capillarity. Clarendon Press, Oxford (1982)
Yue, P., Feng, J.J., Liu, C., Shen, J.: A Diffuse-interface method for simulating two-phase flows of complex fluids. J. Fluid Mech. **515**, 293–317 (2004)